◆ Human Brain Mapping 37:1051–1065 (2016) ◆

Individualized Covariance Profile of Cortical Morphology for Auditory Hallucinations in First-Episode Psychosis

Je-Yeon Yun,[1] Sung Nyun Kim,[1] Tae Young Lee,[2] Myong-Wuk Chon,[1] and Jun Soo Kwon[1,2,3]*

[1]*Department of Psychiatry, Seoul National University College of Medicine, Seoul, Republic of Korea*
[2]*SNU-MRC, Institute of Human Behavioral Medicine, Seoul, Republic of Korea*
[3]*Department of Brain and Cognitive Sciences, College of Natural Science, Seoul National University, Seoul, Republic of Korea*

Abstract: Neocortical phenotype of cortical surface area (CSA) and thickness (CT) are influenced by distinctive genetic factors and undergo differential developmental trajectories, which could be captured using the individualized cortical structural covariance (ISC). Disturbed patterns of neocortical development and maturation underlie the perceptual disturbance of psychosis including auditory hallucination (AH). To demonstrate the utility of selected ISC features as primal biomarker of AH in first-episode psychosis (FEP) subjects experiencing AH (FEP-AH), we employed herein a support vector machine (SVM). A total of 147 subjects (FEP-AH, $n = 27$; FEP-NAH, $n = 24$; HC, $n = 96$) underwent T_1-weighted magnetic resonance imaging at 3T. The FreeSurfer software suite was used for cortical parcellation, with the CSA-ISC and CT-ISC then calculated. The most informative ISCs showing statistical significance ($P < 0.001$) across every run of leave-one-out group-comparison were aligned according to the absolute value of averaged t-statistics and were packaged into candidate feature sets for classification analysis using the SVM. An optimal feature set comprising three CSA-ISCs, including the intraparietal sulcus, Broca's complex, and the anterior insula, distinguished FEP-AH from FEP-NAH subjects with 83.6% accuracy (sensitivity = 82.8%; specificity = 85.7%). Furthermore, six CT-ISCs encompassing the executive control network and Wernicke's module classified FEP-AH from FEP-NAH subjects with 82.3% accuracy (sensitivity = 79.5%; specificity = 88.6%). Finally, extended sets of ISCs related to the default-mode network distinguished FEP-AH or FEP-NAH from HC subjects with 89.0–93.0% accuracy (sensitivity = 88.4–93.4%; specificity = 89.0–94.1%). This study established a distinctive intermediate phenotype of biological proneness for AH in FEP using CSA-ISCs as well as a state marker of disease progression using CT-ISCs. *Hum Brain Mapp 37:1051–1065, 2016.*

Conflict of interest: The authors declare no conflict of interest.
Contract grant sponsor: National Research Foundation of Korea (NRF) funded by the Korean Government (MSIP); Contract grant number: 2015R1A5A7037676.

*Correspondence to: Prof. Jun Soo Kwon, Department of Psychiatry, Seoul National University College of Medicine & Department of Brain & Cognitive Science, College of Natural Science, Seoul National University, 101 Daehak-no, Jongno-gu, Seoul 03080, Republic of Korea. E-mail: kwonjs@snu.ac.kr

Received for publication 1 May 2015; Revised 8 October 2015; Accepted 2 December 2015.
DOI: 10.1002/hbm.23083
Published online 17 December 2015 in Wiley Online Library (wileyonlinelibrary.com).

Key words: auditory hallucination; first-episode psychosis; cortical surface area; cortical thickness; structural covariance; support vector machine

INTRODUCTION

Auditory hallucinations (AH), which are experienced by 60–70% of subjects with schizophrenia [Andreasen and Flaum, 1991; Cachia et al., 2015], may be characterized as false perceptions of sounds including words, whole sentences, or entire conversations in the absence of an identifiable, external stimulus [Jardri et al., 2011, 2013]. Unlike nonclinical subjects who may experience isolated, infrequent AH [van Lutterveld et al., 2014], in subjects with schizophrenia, AH disrupts the thought content and reality-testing capacity of patients, resulting in severe functional impairment in academic, occupational and interpersonal relationship domains, typically during the most productive years of adulthood [Fletcher and Frith, 2009; Shergill et al., 2001]. Furthermore, in 25–30% of psychotic subjects, AH is not resolved satisfactorily by antipsychotic medication [Shergill et al., 2001].

Core schizophrenia symptoms, including AH, may be better understood in the context of dysconnectivity between hub regions, rather than deficits in particular brain areas [Benetti et al., 2015; Rubinov et al., 2009]: AH in schizophrenia might result from crosstalk between hubs comprising distributed, intrinsic brain networks, developed and influenced by both genetic and environmental factors across the neurodevelopmental and maturational phases of structural brain-wiring [Buckholtz and Meyer-Lindenberg, 2012]. Alterations in the perisylvian language network, which produces and interprets semantic information and consists of Broca's area in left inferior frontal cortex and Wernicke's posterior temporal and Geschwind's supramarginal cortices [Catani et al., 2011; Tomasi and Volkow, 2012], have been reported in schizophrenia patients experiencing AH [Benetti et al., 2015; Jardri et al., 2011, 2013]. Furthermore, the close-to-ordinary perceptual nature of AH, which renders discrimination from external sources problematic [Jardri et al., 2011], may be explained by faulty attribution of agency from the self, comediated by the right intraparietal sulcus (IPS) of the dorsal top-down attention network [Anderson et al., 2010] and the anterior insula of the salience network [Ffytche and Wible, 2014; Seeley et al., 2007]. Alterations in the pattern of communication between the salience (SN), executive control (ECN) [Seeley et al., 2007] and default mode (DMN) [Andrews-Hanna et al., 2010] networks also represent a possible neural mechanism underlying AH [Chen et al., 2013; Menon, 2011]. However, cross-sectional studies of alterations in structural and functional connectivity cannot address the fundamental mechanism underlying the erroneous information processing that characterizes AH, which in turn is related to neurodevelopmental and neuromaturational processes in the cerebral cortex [Kubera et al., 2014; Modinos et al., 2009].

Individualized structural covariance (ISC) of cortical morphology, such as cortical surface area (CSA-ISC) and thickness (CT-ISC), represents a concept adapted from interindividual structural covariance [Alexander-Bloch et al., 2013a; Sanabria-Diaz et al., 2010] and intraindividual cortical morphological features [Wee et al., 2013]. ISC describes the inter-regional brain networks per subject reflecting the coordinated growth of brain [Valk et al., 2015], which was influenced by both genetic and environmental factors [Hill et al., 2010; Zielinski et al., 2010] during neurodevelopment [Haukvik et al., 2014] and cortical maturation in adolescence [Alexander-Bloch et al., 2013b] as well as disease-related cortical changes during the progression from prodromal to full-blown psychosis [Wheeler et al., 2014]. CSA and CT are characterized by distinctive developmental trajectories and patterns of variability, influenced by genetic factors and disease-related pathophysiological mechanisms [Haukvik et al., 2014; Kremen et al., 2013]. To facilitate the translation of hypothesized neural mechanisms underlying AH in schizophrenia to individually targeted therapeutic interventions, we employed herein a supervised machine learning strategy, performed using a support vector machine (SVM), to distinguish subjects experiencing AH during first-episode psychosis (FEP-AH) from non-AH FEP subjects (FEP-NAH) and healthy controls (HCs). Notably, we employed the concepts of CSA-ISC and CT-ISC, which incorporate the inherently interconnected nature of cortical morphology at the individual level [Kambeitz et al., 2015], into our SVM model.

MATERIALS AND METHODS

Subjects

A total of 147 participants (FEP, $n = 51$; HCs, $n = 96$) between 17 and 37 years of age, with intelligence quotients (IQ) between 70 and 130 at the time of study enrollment (indexed by the Korean version of the Wechsler Adult Intelligence Scale; K-WAIS) [Yum et al., 1992] and with no prior history of significant head injury, were recruited between May 2010 and October 2014. All 51 FEP patients were recruited from the Seoul Youth Clinic of Seoul National University Hospital and were assessed by certified psychiatrists using the Structured Clinical Interview for DSM-IV axis I Disorders (Patient Edition; SCID-I). Schizophrenia ($n = 31$), schizophreniform disorder ($n = 12$), schizoaffective disorder ($n = 3$), and psychotic disorders not otherwise specified ($n = 5$) represented subjects'

primary axis I psychiatric diagnoses, based on DSM-IV criteria (4th edition, text revision; DSM-IV-TR). In addition, 96 HCs matched with FEP patient for age and sex and recruited using study advertisements were screened using the nonpatient version of the SCID (SCID-NP) to confirm the absence of a lifetime history of psychiatric disorder.

Additional quantitative assessments of psychopathology in FEP subjects, using the Positive and Negative Syndrome Scale (PANSS) [Kay et al., 1987], Hamilton Rating Scale for Depression (HAM-D) [Zimmerman et al., 2013], Hamilton Anxiety Rating Scale (HAM-A) [Bruss et al., 1994], and Modified Global Assessment of Functioning Scale (GAF-M) [Hall, 1995], measured the severity of positive, negative and disorganized symptoms [Edgar et al., 2014] as well as the severity of any accompanying depressive mood, anxiety and the level of functioning, respectively. According to the presence (PANSS P3 $\geq$ 4) or absence (PANSS P3 $\leq$ 2) of AH symptomatology, subjects were allocated to FEP-AH (n = 27) or FEP-NAH (n = 24) subgroups for subsequent analyses.

This study was approved by the Institutional Review Board of Seoul National University Hospital. After receiving a full explanation of the procedures involved, written informed consent was obtained from all participants.

Data Acquisition, Processing, and Extraction of Cortical Morphology

Whole-brain anatomy was measured for all subjects using high-resolution T_1-weighted, three-dimensional Magnetization Prepared Rapid Gradient Echo (TR = 670 ms; TE = 1.89 ms; FOV = 250 mm; FA = 9°; voxel size = 1 × 1 × 1 mm^3) scans on a 3-Tesla scanner (Siemens Magnetom Trio, Erlangen, Germany). CSA and CT were estimated using FreeSurfer software suite (version 5.3.0, http://surfer.nmr.mgh.harvard.edu) [Fischl et al., 2004]. The "recon-all" function of the FreeSurfer suite preprocessed the T1-weighted magnetic resonance imaging (MRI) data within the pipeline consisted of intensity normalization, registration to Talairach space, skull stripping, tissue segmentation, tessellation of the white matter (WM) boundary, smoothing of the tessellated surface and automatic topology correction [Clarkson et al., 2011]. Subsequently, surface deformation processing to define the boundary between WM and pial tissue using the previously tessellated surface as a reference, enabled measurement of CT, calculated as the shortest distance between gray/WM boundary and the gray matter/CSF boundary at each vertex on the tessellated surface [Fischl and Dale, 2000]. After preprocessing of MRI image completed, automatic parcellation with subsequent extraction of the CSA for the 148 regions of interest (ROI) that comprises the 2009 Destrieux atlas was performed [Destrieux et al., 2010].

The signal-to-noise ratio (SNR) of gray-to-WM for each T1WI MRI data [calculated using the "wm-anat-snr–s" command] and of gray matter (GM) intensity for each ROIs of 2009 Destrieux atlas [measured using the "mri_segstats–snr" command] demonstrated relative homogeneity of T1WI acquisition quality [SNR of gray-to-WM; Mean ± SD = 21.94 ± 2.32] and of regional SNR across cortical ROIs [SNR calculated as mean/SD of GM intensity across vertices comprising each ROI; Mean ± SD = 3.79 ± 0.89]. Additional statistical analyses to investigate the correlation between the size or variation of given ROI versus regional SNR of GM intensity did not demonstrate statistical significance for size [mean value of z-scored CSA across the whole 147 subjects vs. regional SNR of GM intensity; Pearson's correlation coefficient = −0.125, P = 0.129] nor for variation [regional SNR of GM intensity vs. standard deviation of z-scored CSA (Pearson's correlation coefficient = 0.0043, P = 0.959) or cortical thickness (Pearson's correlation coefficient = 0.016, P = 0.847) across the whole 147 subjects] of given ROI. After thorough visual inspection of the final processed brain images using the *tkmedit* and *tksurfer* for tissue segmentation, surface reconstruction, and cortical parcellation (with no significant errors detected in any of the 147 subjects), automatically computed CSA and CT values were then extracted and used to calculate ISC networks.

CSA and Thickness-Based ISC

By applying $CSA_k(i)$ and $CT_k(i)$ (normalized regional CSA or CT ROI(i) values in subject k, obtained by dividing the CSA raw-score or CT value by total CSA or average CT values across the cerebral hemisphere in each subject), we regressed-out interindividual cerebral hemispheric size differences from cortical morphological values [Kremen et al., 2013]. Thereafter, we calculated the CSA-ISC or CT-ISC value, of ROI(i) vs. ROI(j) for subject k ($CSA\_ISC_k(i,j)$ or $CT\_ISC_k(i,j)$, respectively; subject k could be either FEP or HC) using the following formula [Wee et al., 2013]:

$$CSA\_ISC_k(i,j) = 1/\exp\left((CSA\_zscored_k(i) - CSA\_zscored_k(j))^2\right)$$

$$CT\_ISC_k(i,j) = 1/\exp\left((CT\_zscored_k(i) - CT\_zscored_k(j))^2\right)$$

where $CSA\_zscored_k(i)$ and $CT\_zscored_k(i)$ were computed as

$$CSA\_zscored_k(i) = (CSA_k(i) - CSA_M(i))/CSA_{SD}(i)$$

$$CT\_zscored_k(i) = (CT_k(i) - CT_M(i))/CT_{SD}(i)$$

$CSA_M(i)$ and $CSA_{SD}(i)$ denote the regional mean and standard deviation of CSA in ROI(i) across all HCs (n = 96).

After calculation of the CSA-ISC or CT-ISC values between the 148 numbers of ROIs for each subject, only the most informative ISCs showing statistical significance (uncorrected $P < 0.001$ [two-tailed], independent t-tests)

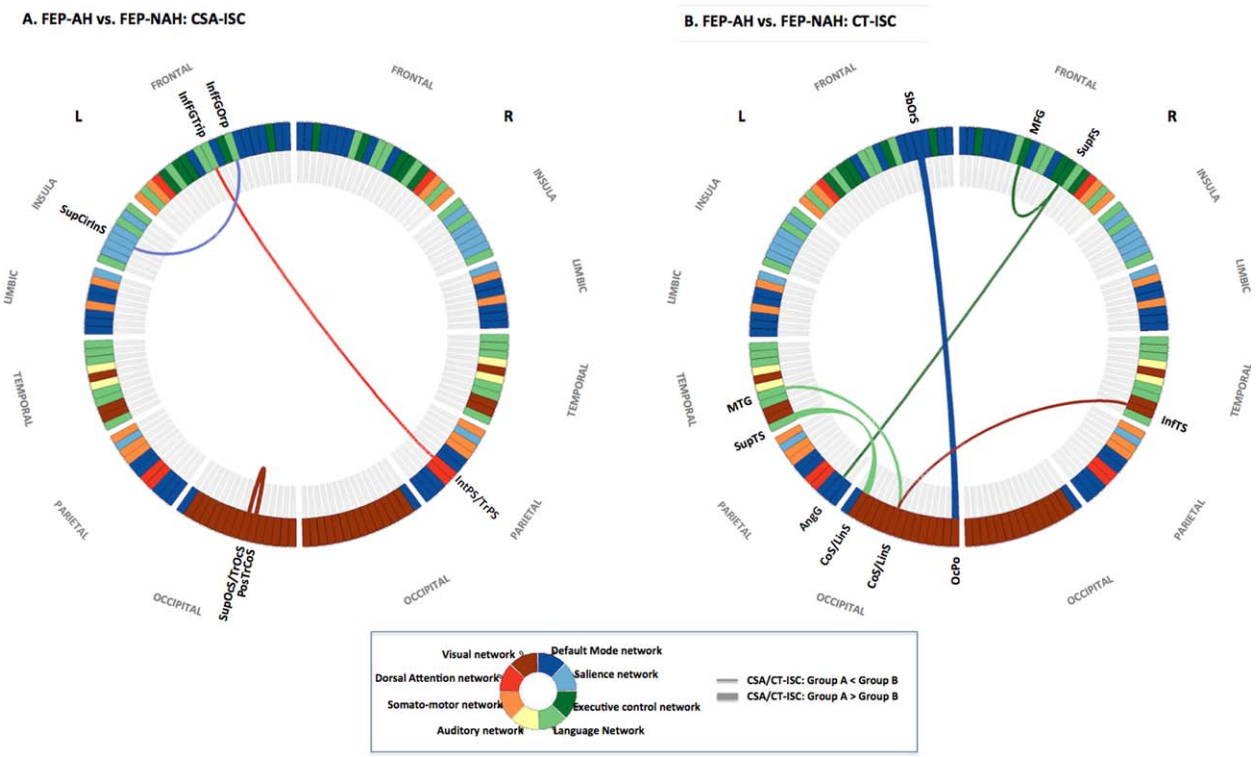

Figure 1.

The optimal neuroanatomical decision function used to classify FEP subject experiencing auditory hallucination (FEP-AH) with FEP subjects without auditory hallucination (FEP-NAH). **(a)** Right IPS-Broca's complex-left anterior insula network of CSA-ISC in FEP-AH. **(b)** ECN-Wernicke's module complex of CT-ISC in FEP-AH. Abbreviations: AngG, angular gyrus; CoS/LinS, medial occipito-temporal sulcus and lingual sulcus; InfFGOrp, pars orbitalis; InfFGTrip, pars triangularis; InfTS, inferior temporal sulcus; IntPS/TrPS, intraparietal sulcus and transverse parietal sulci; L, left hemisphere; MFG, middle frontal gyrus; MTG, middle temporal gyrus; OcPo, occipital pole; PosTrCoS, posterior transverse collateral sulcus; R, right hemisphere; SbOrS, suborbital sulcus; SupCirInS, superior segment of the circular sulcus of the insula; SupFS, superior frontal sulcus; SupOcS/TrOcS, superior and transverse occipital sulcus; SupTS, superior temporal sulcus. [Color figure can be viewed in the online issue, which is available at wileyonlinelibrary.com.]

across every n runs of leave-one-out group-comparison (n = 51 for FEP-AH vs. FEP-NAH; n = 123 for FEP-AH vs. HC; n = 120 for FEP-NAH vs. HC) [Dosenbach et al., 2010] were aligned according to the absolute value of averaged t-statistics and were packaged into candidate feature sets (S_CSA_group-A_group-B(k/n) or S_CT_group-A_group-B(k/n), $1 \leq k \leq n$, n = maximum number of candidate feature) for classification analysis using SVM method.

SVM: Classification of FEP-AH versus FEP-NAH or HC

All SVM (using the nonlinear radial basis function kernel [sigma = 2] with a constant soft-margin [cost = 1]) training, testing and iterative group separation procedures (with random permutation of subjects into training and testing sets for cross-validation) were performed using the Statistics Toolbox of the Matlab software package (ver. R2014b; MathWorks, Natick, MA) and repeated 10,000 times per candidate feature set. The most accurate group classifier, evidenced by its highest overall mean accuracy **across the 10,000 cross-validation procedures** ($P < 0.001$, two-tailed and Bonferroni-corrected; independent t-test) [Yun et al., 2015], was referred to as "neuroanatomical decision functions of SVM (Figs. 1–3 and Tables III–V; visualization created using Circos [Irimia et al., 2012; Krzywinski et al., 2009])."

In the SVM training procedure to distinguish FEP-AH from FEP-NAH, using a training dataset of 41 subjects collected from the 51 total FEPs (random permutation method), the decision boundary constructed using a candidate feature set (S_CSA_FEP-AH_FEP-NAH(k/n)) or S_CT_FEP-AH_FEP-NAH(k/n)) was optimized to maximize group classification accuracy. During the testing phase, using a test dataset of 10 FEPs not disclosed in the SVM training phase, the decision solution for a given

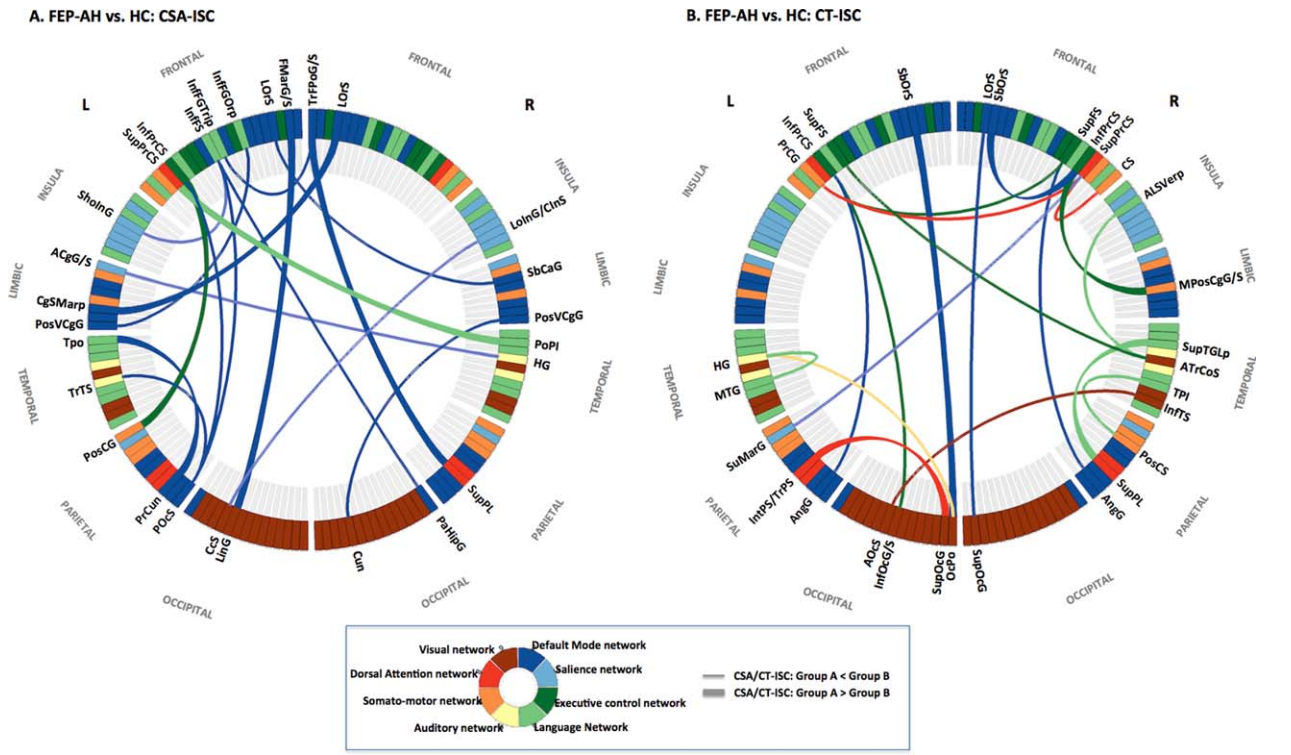

Figure 2.

The optimal neuroanatomical decision function used to classify FEP subject experiencing auditory hallucination (FEP-AH) with HC. **(a)** Altered pattern of CSA-ISC in FEP-AH: intranetwork ISC of DMN as well as inter-network ISC between DMN and perisylvian language network. **(b)** Distorted pattern of CT-ISC in FEP-AH: internetwork ISCs between the DMN versus ECN as well as between the language network versus other primary sensory networks. **Abbreviations**: ACgG/S, anterior part of the cingulate gyrus and sulcus; ALSVerp, vertical ramus of the anterior segment of the lateral sulcus; AngG, angular gyrus; AOcS, anterior occipital sulcus; ATrCoS, anterior transverse collateral sulcus; CcS, calcarine sulcus; CgSMarp, marginal branch of the cingulate sulcus; CS, central sulcus; Cun, cuneus; FMarG/S, frontomarginal gyrus and sulcus; HG, Heschl's gyrus; InfFGOrp, pars orbitalis; InfFGTrip, pars triangularis; InfFS, inferior frontal sulcus; InfOcG/S, inferior occipital gyrus and sulcus; InfPrCS, inferior part of the precentral sulcus; InfTS, inferior temporal sulcus; IntPS/TrPS, intraparietal sulcus and transverse parietal sulci; L, left hemisphere; LinG, lingual gyrus; LoInG/ClnS, long insular gyrus and central insular sulcus; LOrS, lateral orbital sulcus; MPosCgG/S, middle-posterior part of the cingulate gyrus and sulcus; MTG, middle temporal gyrus; OcPo, occipital pole; PaHipG, parahippocampal gyrus; POcS, parieto-occipital sulcus; PoPI, planum polare; PosCG, postcentral sulcus; PosCS, postcentral sulcus; PoSVCgG, posterior-ventral part of the cingulate gyrus; PrCG, precentral gyrus; PrCun, precuneus; R, right hemisphere; SbCaG, subcallosal gyrus; SbOrS, suborbital sulcus; ShoInG, short insular gyrus; SuMarG, supramarginal gyrus; SupFS, superior frontal sulcus; SupOcG, superior occipital gyrus; SupPL, superior parietal lobule; SupPrCS, superior part of the precentral sulcus; SupTGLp, lateral aspect of the superior temporal gyrus; TPI, planum temporale; Tpo, temporal pole; TrTS, transverse temporal sulcus. [Color figure can be viewed in the online issue, which is available at wileyonlinelibrary.com.]

observation x ($1 \leq x \leq 10$), based on a set of candidate features was calculated [Dosenbach et al., 2010]. During the SVM model training and testing phase, to distinguish HCs from FEP-AH or FEP-NAH subjects separately, random preselection of HCs (n = 27 for FEP-AH vs. HC, n = 24 for FEP-NAH vs. HC) preceded the division of subjects into 44 (for FEP-AH vs. HC) or 38 (for FEP-NAH vs. HC) training subjects and 10 testing subjects [van Waarde et al., 2015].

RESULTS

Demographic and Clinical Data

The demographic and clinical characteristics of the subjects are described in Table I. There were no significant group differences in age, sex or the socio-economic status of parents among the FEP-AH, FEP-NAH, and HC groups ($P > 0.05$, two-tailed, one-way analysis of variance). However, there was a difference between the IQ scores of the

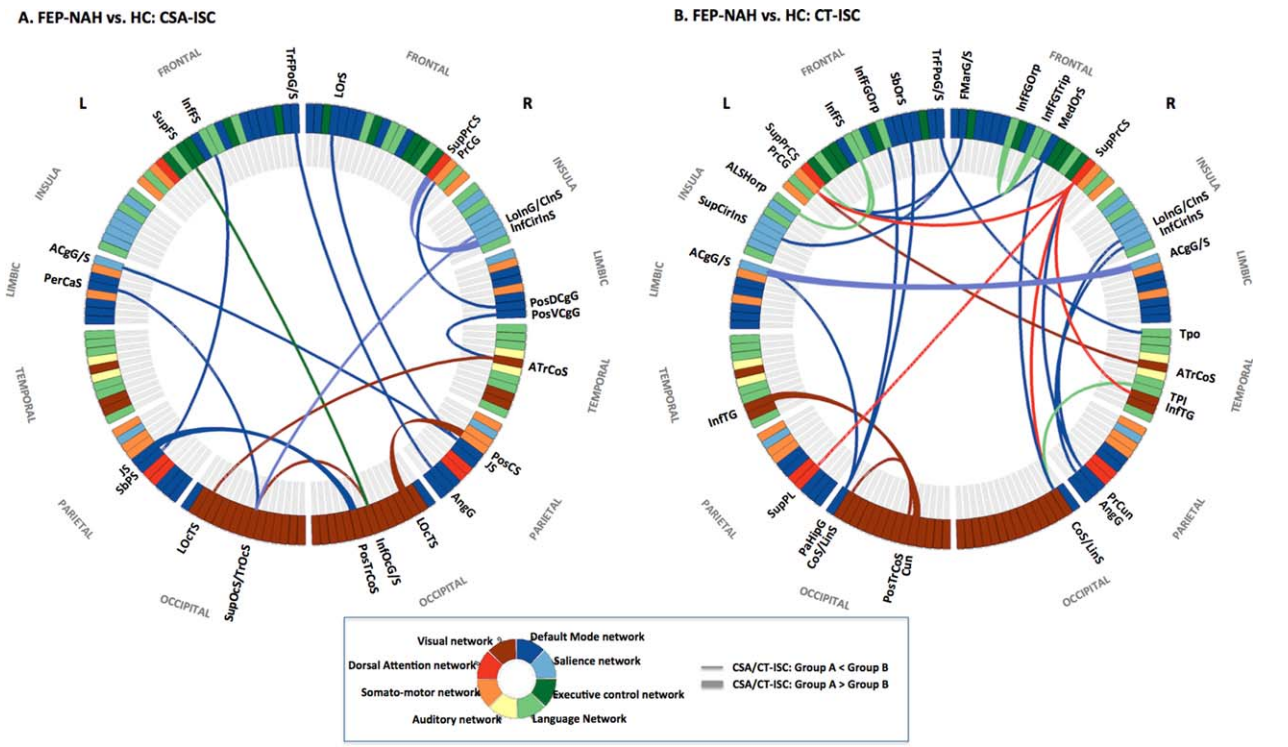

Figure 3.

The optimal neuroanatomical decision function used to classify FEP subject without auditory hallucination (FEP-NAH) with HC. **(a)** Changed pattern of CSA-ISC in FEP-NAH: intra-network ISC of DMN as well as inter-network ISC between DMN versus visual, somato-motor, salience and perisylvian language networks. **(b)** Differential pattern of CT-ISC in FEP-NAH: intranetwork ISC of DMN as well as internetwork ISCs between the DMN versus salience and language networks. **Abbreviations**: ACgG/S, anterior part of the cingulate gyrus and sulcus; ALSHorp, horizontal ramus of the anterior segment of the lateral sulcus; AngG, angular gyrus; ATrCoS, anterior transverse collateral sulcus; CoS/LinS, medial occipital-temporal and lingual sulcus; Cun, cuneus; FMarG/S, fronto-marginal gyrus and sulcus; InfCirIns, inferior segment of the circular sulcus of insula; InfFGOrp, pars orbitalis; InfFGTrip, pars triangularis; InfFS, inferior frontal sulcus; InfOcG/S, inferior occipital gyrus and sulcus; InfTG, inferior temporal gyrus; JS, sulcus intermedius primus; LOcTS, lateral occipito-temporal sulcus; LoInG/ClnS, long insular gyrus and central insular sulcus; LOrS, lateral orbital sulcus; MedOrS, medial orbital sulcus; PaHipG, parahippocampal gyrus; PerCaS, pericallosal sulcus; PosCS, postcentral sulcus; PosDCgG, posterior-dorsal part of the cingulate gyrus; PosTrCoS, posterior transverse collateral sulcus; PosVCgG, posterior-ventral part of the cingulate gyrus; PrCG, precentral gyrus; PrCun, precuneus; SbOrS, suborbital sulcus; SbPS, subparietal sulcus; SupCirInS, superior segment of the circular sulcus of the insula; SupFS, superior frontal sulcus; SupOcS/TrOcS, superior and transverse occipital sulcus; SupPL, superior parietal lobule; SupPrCS, superior part of the precentral sulcus; TPI, planum polare; Tpo, temporal pole; TrFPoG/S, transverse frontopolar gyrus and sulcus. [Color figure can be viewed in the online issue, which is available at wileyonlinelibrary.com.]

FEP and HC groups ($P < 0.001$), which may reflect an increased risk of psychosis commensurate with lower intelligence, even during the premorbid stage [Meier et al., 2014]. Furthermore, compared with HCs, the educational level of the FEP-AH group was also lower ($P < 0.001$).

There were no differences between the FEP-AH and FEP-NAH subgroups in terms of statistically for age of onset, duration of illness, GAF-M scores 1 year prior to study inclusion, IQ scores or negative symptom factor score of psychosis [Edgar et al., 2014] measured at enrollment ($P > 0.05$, two-tailed, independent t-test). The duration of use and dose (converted into chlorpromazine-equivalent doses [Woods, 2003]) of antipsychotics before MRI did not differ between the FEP-AH and FEP-NAH groups (all $P > 0.05$, independent t-test). However, there were differences between these two groups in terms of positive symptom factor scores, total PANSS scores and degree of functional impairment at enrollment measured using the GAF-M (all $P < 0.001$, two-tailed).

TABLE I. Demographic and clinical characteristics of subjects with FEP and HC subjects[a]

Characteristics	FEP-AH [PANSS P3 ≥ 4] (n = 27)		FEP-NAH [PANSS P3 ≤ 2] (n = 24)		HC (n = 96)		Statistics		
	Mean	SD	Mean	SD	Mean	SD	$\chi^2/T/F$	df	P value
Age (years)[b]	22.48	4.95	22.69	5.12	24.07	4.84	1.167	144	0.314
Sex (Male/Female)[a]	9/18		12/12		57/39		5.846	2	0.054
Years of Education (years)[b,c]	12.85	1.97	13.92	1.94	14.36	1.69	7.66	143	<0.001[d]
IQ[b]	97.33	14.25	100.29	11.64	111.76	10.62	21.74	144	<0.001[d,e]
Socio-Economic Status of Parents[b,f]	2.63	0.84	2.58	0.97	2.81	0.88	0.85	137	0.43
Age at Onset (years)[g]	22	4.97	23.54	4.45			−1.169	48.99	0.248
Duration of Illness (years)[g]	0.6	0.52	0.73	0.47			−0.888	48.97	0.379
Duration of Antipsychotics Usage Before MRI scanning (years)[g]	0.09	0.16	0.18	0.23			−1.576	40.31	0.123
Antipsychotics Treatment at MRI Scanning (CPZ equivalent, mg/day)[g]	327.47	522.24	238.02	225.96			0.809	36.28	0.424
Positive and negative symptom scale for schizophrenia (PANSS)[g]									
Positive symptom factor score (P1, P3, P5-6, N7, G1, G9, G12)	22.81	5.42	16.96	4.76			4.108	49	<.001
Negative symptom factor score (N1-4, N6-7, G16)	18.81	6.02	16.58	4.84			1.466	48.54	.149
Disorganized symptom factor score (P2, N5, G5, G10-11, G13, G15)	15.3	4.8	12.33	3.71			2.479	48.13	.017
Total score	73.0	13.90	59.71	12.78			3.556	48.94	<.001
HAM-D[g]	10.19	3.54	9.88	5.74			0.229	37.43	.82
HAM-A[g]	8.59	4.43	7.33	3.84			1.087	48.97	.282
Modified GAF-M[g]									
At Intake	41.67	8.59	51.63	10.45			−3.691	44.68	<.001
One Year Prior to Intake	67.7	12.27	72.04	10.74			−1.346	48.99	.184

Abbreviations: AH, auditory hallucination; CPZ, Chlorpromazine; FEP, first-episode psychosis; MRI, magnetic resonance imaging.
[a]Differences between variables of three groups were assessed using chi-squared test.
[b]Differences between variables of three groups were assessed using analysis of variance test.
[c]For 1 case of HC, information was missing.
[d]Statistically significant group difference between FEP-AH versus HC ($p < .05$).
[e]Statistically significant group difference between FEP-NAH versus HC ($p < .05$).
[f]For seven cases of HC, information was missing.
[g]Differences between variables of two groups were assessed using independent t-test.

Neuroanatomical Decision Function of CSA-ISC or CT-ISC: FEP-AH versus FEP-NAH

For the three largest CSA-ISCs (Table III and Fig. 1A), ranked according to the mean t-statistics derived from the consensus feature list of four total candidate features, FEP-AH and FEP-NAH subjects were distinguished with a mean accuracy of 83.61% (sensitivity = 82.84%; specificity = 85.66%; Table II). Decreased CSA-ISCs between the right IPS versus left pars triangularis as well as between the left pars orbitalis versus the left superior segment of the circular sulcus of the insula, and increased CSA-ISCs between the left posterior transverse collateral sulcus versus the left transverse occipital sulcus represented the key characteristics distinguishing FEP-AH from FEP-NAH subjects [Chi et al., 1977].

A set of explanatory features, comprising all six CT-ISCs (Table III and Fig. 1B) classified the FEP subjects as FEP-AH or FEP-NAH with a mean accuracy of 82.30% (sensitivity = 79.48%; specificity = 88.64%; **Table** II). In the dorsolateral prefrontal cortex (DLPFC), decreased CT-ISCs between the right superior frontal sulcus versus right superior frontal sulcus and left angular gyrus indicated their role in distinguishing FEP-AH from FEP-NAH subjects. Furthermore, FEP-AH subjects also exhibited changed CT-ISC compared with FEP-NAH in the left middle temporal gyrus versus left anterior occipital sulcus as well as in the left superior temporal sulcus versus left medial occipito-temporal sulcus. Notably, the increased CT-ISC between the left occipital pole versus left medial prefrontal cortex (suborbital sulcus), and the decreased CT-ISC between the right inferior temporal sulcus versus

TABLE II. Averaged group classification performance–over the 10,000 times of iterative process composed of random permutations (to split the two groups combined into (*n*-10; *n* = 51 for FEP-AH vs. FEP-NAH, *n* = 123 for FEP-AH vs. HC, *n* = 120 for FEP-NAH vs. HC) training subjects vs. 10 testing subjects) with subsequent group classification using the SVM-of the optimal feature set of SVM group classifier (neuroanatomical decision function)

	FEP-AH vs. FEP-NAH[a]		FEP-AH vs. HC[b]		FEP-NAH vs. HC[c]	
Binary classifier	Mean	SD	Mean	SD	Mean	SD
CSA-ISC						
True positive	4.62	1.34	4.64	1.36	4.50	1.36
True negative	3.74	1.30	4.51	1.38	4.40	1.37
False positive	0.98	0.89	0.48	0.69	0.62	0.79
False negative	0.66	0.82	0.37	0.62	0.48	0.72
Sensitivity (%)	82.84	15.65	90.96	13.30	88.38	14.74
Specificity (%)	85.66	17.41	92.51	12.69	90.52	14.17
Accuracy (%)	83.61	10.91	91.52	8.53	88.99	9.71
Positive predictive value (%)	88.13	14.20	93.15	11.57	90.97	13.51
Negative predictive value (%)	79.99	17.74	90.96	13.16	88.30	14.91
CT-ISC						
True positive	4.78	1.32	4.42	1.39	4.71	1.38
True negative	3.45	1.27	4.68	1.41	4.58	1.39
False positive	1.27	0.99	0.32	0.56	0.42	0.65
False negative	0.50	0.77	0.58	0.70	0.29	0.52
Sensitivity (%)	79.48	15.53	93.35	11.89	92.07	12.57
Specificity (%)	88.64	17.04	88.99	13.57	94.12	10.90
Accuracy (%)	82.30	10.65	90.97	8.49	92.95	7.75
Positive predictive value (%)	91.39	13.04	88.69	13.87	94.60	9.94
Negative predictive value (%)	73.88	19.39	93.88	10.81	92.06	12.41

Abbreviations: FEP, first episode psychosis; AH, auditory hallucination; NAH, without auditory hallucination; HC, healthy control; CT, cortical thickness; ISC, correlative morphological features; CSA, cortical surface area; K, feature ranking; SD, standard deviation.

the left anterior occipital sulcus, together represented the key characteristics distinguishing FEP-AH from FEP-NAH and HC subjects.

Neuroanatomical Decision Function of CSA-ISC or CT-ISC: FEP-AH versus HC

An optimum feature set comprising 17 CSA-ISCs (Table IV and Fig. 2A), which ranked the 20 significance results according to averaged t-statistics, successfully distinguished FEP-AH from HC subjects with a mean accuracy of 91.52% (sensitivity = 90.96%; specificity = 92.51%; Table II). Compared with HCs, FEP-AH subjects exhibited altered strength of CSA-ISCs in the left inferior frontal and right transverse frontopolar cortices as well as in the left parieto-occipital sulcus with other brain regions. In addition, another optimal feature set comprising 19 CT-ISCs (Table IV and Fig. 2B), which ranked 22 CT-ISCs, successfully distinguished FEP-AH from HC subjects with a mean accuracy of 90.97% (sensitivity = 93.35%; specificity = 88.99%; Table II). Specifically, the right superior frontal sulcus of the DLPFC, bilateral precentral sulci, the right anterior transverse collateral sulcus and left occipital pole exhibited changed CT-ISCs with other prefronto-temporal regions. Notably, decreased CT-ISC between left precentral gyrus and right superior precentral sulcus was simultaneously ranked as a component of optimal feature sets each classifying HC from FEP-AH or from FEP-NAH.

Neuroanatomical Decision Function of CSA-ISC or CT-ISC: FEP-NAH versus HC

An optimal feature set comprising 14 CSA-ISCs (Table V and Fig. 3A) distinguished FEP-NAH from HC subjects with a mean accuracy of 88.99% (sensitivity = 88.38%; specificity = 90.52%; Table II). In FEP-NAH subjects, differential strength in CSA-ISC of the right sulcus intermedius primus and anterior transverse collateral sulcus, left transverse occipital sulcus and the right inferior occipital cortex with other midline and posterior brain regions worked as effective explanatory features in group classification of FEP-NAH versus HC. However, 23 optimal explanatory features of CT-ISCs (Table V and Fig. 3B) selected from the 24 total candidate CT-ISCs distinguished FEP-NAH from HC with a mean accuracy of 92.95% (sensitivity = 92.07%; specificity = 94.12%; Table II). In other words, several CT-ISCs between the right superior precentral sulcus, right medial occipito-temporal sulcus, left precentral and parahippocampal gyrus versus other

TABLE III. Optimal feature set (neuroanatomical decision function) of SVM model achieving the highest accuracy of classification for first-episode psychosis subjects into FEP-AH or FEP-NAH

No.	ROI_I_name	ROI_J_name	T stat [LOOGC] mean	FEP-AH ($N = 27$), mean (SD)	FEP-NAH ($N = 24$), mean (SD)	HC ($N = 96$), mean (SD)
CSA- ISC: FEP-AH vs. FEP-NAH						
1	Right IPS	Left pars triangularis	−4.496	0.19 (0.29)	0.60 (0.35)	0.44 (0.38)
2	Left posterior transverse collateral sulcus (ptCoS: hV4/VO1 boundary)	Left transverse occipital sulcus (scene-selective TOS)	4.239	0.59 (0.35)	0.19 (0.31)	0.46 (0.36)
3	Left pars orbitalis	Left superior segment of the circular sulcus of the insula	−3.751	0.23 (0.28)	0.56 (0.34)	0.45 (0.36)
CT- ISC: FEP-AH vs. FEP-NAH						
1	Right superior frontal sulcus	Left angular gyrus	−4.035	0.30 (0.32)	0.67 (0.32)	0.45 (0.36)
2	Left middle temporal gyrus	Left anterior occipital sulcus [hOc5, motion-sensitive area (V5/MT+)]	−3.853	0.28 (0.36)	0.67 (0.36)	0.44 (0.36)
3	Left occipital pole	Left suborbital sulcus	3.809	0.70 (0.36)	0.32 (0.34)	0.37 (0.34)
4	Right inferior temporal sulcus (Extrastriate Body Area)	Left anterior occipital sulcus [hOc5, motion-sensitive area (V5/MT+)]	−3.748	0.23 (0.28)	0.57 (0.34)	0.50 (0.36)
5	Left medial occipito-temporal sulcus	Left superior temporal sulcus	3.71	0.57 (0.30)	0.26 (0.28)	0.46 (0.38)
6	Right middle frontal gyrus	Right superior frontal sulcus	−3.681	0.33 (0.33)	0.68 (0.33)	0.50 (0.36)

Abbreviations: FEP-AH, first episode psychosis with auditory hallucination; FEP-NAH, first episode psychosis without auditory hallucination; HC, healthy control; LOOGC, leave-one-out group-comparison; L, left; R, Right.

brain regions were distorted in FEP-NAHs compared with HCs.

DISCUSSION

To the best of our knowledge, this is the first study to unravel the individualized neural mechanisms underlying AH in FEP in the context of CSA- and CT-based structural covariance calculated per each subject. In this study, a SVM classification model, using an optimal feature set comprising three CSA-ISCs, distinguished FEP-AH from FEP-NAH subjects with a mean accuracy of 83.61%. Because CSA changes only marginally across the prodromal and full-blown stages of psychosis [Gutierrez-Galve et al., 2015a], and major symptom dimensions such as AH that begun during FEP tend to remain stable even after 5–10-years of follow-up [Russo et al., 2014], differences in CSA-ISCs between the right IPS, Broca's complex (left pars triangularis and pars orbitalis) [Xiang et al., 2010], and left circular sulcus of the anterior insula may represent genetically laden, subtle deviation of coordinated cortical development process from normal, thereby conferring biological proneness to AH symptomatology in psychosis [Hill et al., 2010; Zielinski et al., 2010]. Another SVM classification model, using an optimal feature set comprising the six CT-ISCs that encompass the ECN-Wernicke's module [Seeley et al., 2007; Tomasi and Volkow, 2012], distinguished FEP-AH from FEP-NAH subjects with 82.3% accuracy, thereby demonstrating the clinical value of CT changes as a state marker of executive function maturation and the progression of psychiatric disorders including schizophrenia [Cannon et al., 2015]. Finally, extended sets of ISCs which illustrate changed crosstalk between the DMN versus other intrinsic brain networks as well as between the two DMN subnetworks [Bastos-Leite et al., 2015] distinguished FEP-AH or FEP-NAH from HC subjects with a mean accuracy range of 89.0–93.0%.

Right IPS-Broca's Complex-Anterior Insula Network of CSA-ISCs in FEP-AH

Three CSA-ISCs at the intersection of attentional control and self-agency for semantic content according to the salience of which successfully characterized neural cortical

TABLE IV. Optimum feature set (neuroanatomical decision function) of SVM model achieving the highest accuracy of classification for fep subjects experiencing auditory hallucination from HC

No.	ROI_I_name	ROI_J_name	T stat [LOOGC] Mean	FEP-AH ($N = 27$), Mean (SD)	FEP-NAH ($N = 24$), Mean (SD)	HC ($N = 96$), Mean (SD)
CSA-ISC: FEP-AH vs. HC						
1	Lt. short insular gyrus	Lt. inferior frontal sulcus	−4.714	0.19 (0.28)	0.25 (0.29)	0.5 (0.35)
2	Lt. inferior frontal sulcus	Lt. parieto-occipital sulcus (visuospatial processing; V6/V6Av/V6Ad)	−4.619	0.17 (0.25)	0.49 (0.36)	0.45 (0.36)
3	Lt. PCC	Lt. pars orbitalis	−4.591	0.20 (0.29)	0.37 (0.39)	0.51 (0.37)
4	Lt. precuneus	Lt. temporal pole	4.389	0.72 (0.31)	0.57 (0.33)	0.42 (0.37)
5	Rt. Heschl's gyrus	Lt. ACC	−4.156	0.25 (0.27)	0.42 (0.35)	0.51 (0.36)
6	Rt. parahippocampal gyrus	Lt. inferior frontal sulcus	−4.123	0.22 (0.29)	0.43 (0.39)	0.50 (0.38)
7	Lt. postcentral gyrus	Lt. inferior precentral sulcus	4.123	0.71 (0.32)	0.48 (0.39)	0.42 (0.35)
8	Rt. frontal pole	Lt. pars triangularis	−4.069	0.26 (0.28)	0.44 (0.37)	0.53 (0.38)
9	Lt. parieto-occipital sulcus (visuospatial processing; V6/V6Av/V6Ad)	Lt. transverse temporal sulcus	−4.015	0.21 (0.25)	0.42 (0.35)	0.46 (0.38)
10	Rt. subcallosal gyrus	Lt. lateral orbital sulcus	−4.012	0.27 (0.31)	0.46 (0.40)	0.55 (0.38)
11	Rt. lateral orbital sulcus	Lt. marginalis branch of the cingulate sulcus	3.985	0.72 (0.29)	0.45 (0.44)	0.45 (0.39)
12	Rt. frontal pole	Rt. superior parietal lobule	3.922	0.68 (0.28)	0.55 (0.36)	0.43 (0.36)
13	Rt. PCC	Rt. cuneus	−3.906	0.25 (0.28)	0.39 (0.39)	0.50 (0.36)
14	Lt. fronto-marginal gyrus/sulcus	Lt. lingual gyrus	3.872	0.72 (0.27)	0.46 (0.36)	0.47 (0.36)
15	Rt. planum polare	Lt. superior precentral sulcus	3.834	0.69 (0.30)	0.48 (0.39)	0.43 (0.34)
16	Rt. long insular gyrus/central sulcus	Lt. calcarine sulcus	−3.813	0.23(0.27)	0.29 (0.35)	0.48 (0.38)
17	Lt. parieto-occipital sulcus (visuospatial processing; V6/V6Av/V6Ad)	Lt. inferior precentral sulcus	−3.803	0.26 (0.28)	0.43 (0.38)	0.51 (0.37)
CT- ISC: FEP-AH vs. HC						
1	Rt. planum temporale	Rt. postcentral sulcus	−4.915	0.26 (0.27)	0.45 (0.32)	0.58 (0.36)
2	Lt. angular gyrus	Rt. superior frontal sulcus	−4.833	0.17 (0.20)	0.49 (0.39)	0.43 (0.37)
3	Lt. inferior occipital gyrus/sulcus	Lt. inferior precentral sulcus	−4.606	0.14 (0.25)	0.40 (0.37)	0.43 (0.39)
4	Rt. superior frontal sulcus	Lt. precentral gyrus	−4.445	0.19 (0.26)	0.40 (0.39)	0.46 (0.35)
5	Lt. angular gyrus	Lt. inferior precentral sulcus	−4.303	0.20 (0.25)	0.49 (0.36)	0.46 (0.36)
6	Lt. occipital pole	Lt. suborbital sulcus	4.277	0.70 (0.36)	0.32 (0.34)	0.37 (0.34)
7	Rt. central sulcus	Rt. superior precentral sulcus	−4.269	0.20 (0.25)	0.41 (0.42)	0.46 (0.37)
8	Rt. superior precentral sulcus	Lt. precentral gyrus	−4.258	0.26 (0.31)	0.26 (0.32)	0.56 (0.37)
9	Rt. inferior temporal sulcus	Lt. anterior occipital sulcus (hOc5, motion-sensitive area (V5/MT+))	−4.037	0.23 (0.28)	0.57 (0.34)	0.50 (0.36)
10	Rt. superior precentral sulcus	Lt. supramarginal gyrus	−4.027	0.22 (0.23)	0.43 (0.36)	0.45 (0.36)
11	Lt. superior occipital gyrus	Lt. IPS	4.01	0.71 (0.31)	0.45 (0.31)	0.43 (0.36)
12	Rt. pMCC	Rt. inferior precentral sulcus	3.918	0.72 (0.32)	0.52 (0.35)	0.44 (0.38)
13	Rt. inferior precentral sulcus	Rt. subobital sulcus	3.917	0.71 (0.30)	0.49 (0.41)	0.44 (0.36)
14	Lt. Heschl's gyrus	Lt. occipital pole	−3.913	0.25 (0.24)	0.29 (0.30)	0.48 (0.37)
15	Rt. vertical ramus of the anterior segment of the lateral sulcus	Rt. anterior transverse collateral sulcus (building related area)	−3.798	0.26 (0.28)	0.52 (0.41)	0.51 (0.37)
16	Rt. superior parietal lobule	Rt. lateral superior temporal gyrus	3.794	0.68 (0.31)	0.56 (0.38)	0.42 (0.35)
17	Rt. anterior transverse collateral sulcus (building related area)	Lt. superior frontal sulcus	−3.783	0.22 (0.32)	0.33 (0.36)	0.50 (0.38)
18	Rt. superior occipital gyrus	Rt. lateral orbital sulcus	−3.776	0.24 (0.28)	0.38 (0.35)	0.49 (0.37)
19	Lt. Heschl's gyrus	Lt. middle temporal gyrus	−3.765	0.24 (0.29)	0.42 (0.37)	0.49 (0.36)

Abbreviations: ACC, anterior cingulate cortex; FEP-AH, first episode psychosis with auditory hallucination; FEP-NAH, first episode psychosis without auditory hallucination; HC, healthy control; LOOGC, leave-one-out group-comparison; L, left; PCC, posterior cingulate cortex; R, Right.

TABLE V. Optimum feature set (neuroanatomical decision function) of SVM model achieving the highest accuracy of classification for FEP subjects without auditory hallucination from HC

No.	ROI_I_name	ROI_J_name	T stat [LOOGC] Mean	FEP-AH ($N = 27$), Mean (SD)	FEP-NAH ($N = 24$), Mean (SD)	HC ($N = 96$), Mean (SD)
CSA-ISC: FEP-NAH vs. HC						
1	Rt. PCC	Left posterior transverse collateral sulcus (ptCoS: hV4/VO1 boundary)	−4.548	0.37 (0.38)	0.17 (0.26)	0.46 (0.38)
2	Lt. inferior frontal sulcus	Lt. subparietal sulcus	−4.485	0.31 (0.36)	0.22 (0.27)	0.52 (0.36)
3	Rt. inferior occipital gyrus/sulcus	Lt. transverse occipital sulcus (scene-selective TOS)	−4.237	0.48 (0.39)	0.19 (0.31)	0.51 (0.36)
4	Lt. transverse occipital sulcus (scene-selective TOS)	**Lt. pericallosal sulcus**	−4.055	0.44 (0.37)	0.16 (0.28)	0.43 (0.37)
5	Rt. Sulcus intermedius primus	Lt. ACC	−4.035	0.30 (0.37)	0.20 (0.27)	0.47 (0.36)
6	Rt. posterior transverse collateral sulcus (ptCoS: hV4/VO1 boundary)	Lt. Sulcus intermedius primus	3.989	0.40 (0.37)	0.72 (0.33)	0.41 (0.37)
7	Rt. inferior occipital gyrus/sulcus	Lt. superior frontal sulcus	−3.977	0.47 (0.37)	0.20 (0.26)	0.46 (0.36)
8	Rt. Sulcus intermedius primus	Rt. Lateral orbital sulcus	−3.95	0.44 (0.42)	0.23 (0.33)	0.54 (0.37)
9	Rt. Inferior segment of the circular sulcus	Rt. superior precentral sulcus	3.946	0.46 (0.33)	0.69 (0.29)	0.42 (0.34)
10	Rt. lateral occipito-temporal sulcus (recognizing face)	Rt. postcentral sulcus	3.945	0.51 (0.35)	0.72 (0.30)	0.43 (0.37)
11	Rt. anterior transverse collateral sulcus (building related area)	Lt. lateral occipito-temporal sulcus (visual word form area)	−3.848	0.43 (0.36)	0.18 (0.26)	0.45 (0.41)
12	Rt. Long insular gyrus and central sulcus	Lt. transverse occipital sulcus (scene-selective TOS)	−3.838	0.36 (0.37)	0.24 (0.21)	0.46 (0.35)
13	Rt. dPCC	Rt. precentral gyrus	−3.775	0.45 (0.38)	0.23 (0.29)	0.50 (0.38)
14	Rt. angular gyrus	Lt. transverse frontopolar gyrus/sulcus	−3.769	0.45 (0.37)	0.24 (0.32)	0.52 (0.38)
CT-ISC: FEP-NAH vs. HC						
1	Rt. medial occipito-temporal sulcus	Rt. superior precentral sulcus	−5.525	0.44 (0.39)	0.15 (0.23)	0.49 (0.38)
2	Rt. temporal pole	Lt. transverse frontopolar gyri and sulci	−5.409	0.49 (0.38)	0.18 (0.26)	0.53 (0.37)
3	Rt. medial orbital sulcus	Lt. precentral gyrus	−5.396	0.32 (0.35)	0.14 (0.20)	0.44 (0.38)
4	Rt. anterior transverse collateral sulcus (building related area)	Lt. precentral gyrus	−4.786	0.41 (0.40)	0.15 (0.23)	0.43 (0.35)
5	Lt. cuneus	Lt. inferior temporal gyrus	4.58	0.55 (0.38)	0.70 (0.28)	0.39 (0.36)
6	Rt. fronto-marginal gyrus/sulcus	Lt. precentral gyrus	−4.528	0.36 (0.42)	0.19 (0.22)	0.45 (0.35)
7	Rt. precuneus	Rt. superior precentral sulcus	−4.511	0.36 (0.37)	0.20 (0.27)	0.51 (0.38)
8	Lt. parahippocampal gyrus	Lt. suborbital sulcus	−4.468	0.45 (0.38)	0.19 (0.23)	0.45 (0.36)
9	Rt. fronto-marginal gyrus/sulcus	Lt. superior segment of the circular sulcus	−4.327	0.42 (0.36)	0.22 (0.25)	0.49 (0.35)
10	Rt. pars orbitalis	Rt. pars triangularis	4.231	0.60 (0.30)	0.73 (0.29)	0.44(0.32)
11	Rt. Long insular gyrus and central sulcus	Rt. Precuneus	−4.214	0.50 (0.37)	0.20 (0.25)	0.47 (0.37)
12	Lt. inferior frontal sulcus	Lt. superior precentral sulcus	−4.213	0.32 (0.34)	0.23 (0.27)	0.51 (0.36)
13	Rt. angular gyrus		−4.165	0.40 (0.35)	0.19 (0.26)	0.46 (0.34)

TABLE V. (continued).

No.	ROI_I_name	ROI_J_name	T stat [LOOGC] Mean	FEP-AH ($N = 27$), Mean (SD)	FEP-NAH ($N = 24$), Mean (SD)	HC ($N = 96$), Mean (SD)
		Rt. inferior segment of the circular sulcus				
14	Rt. planum temporale	Rt. medial occipito-temporal sulcus	−4.136	0.35 (0.39)	0.17 (0.24)	0.42 (0.37)
15	Lt. posterior transverse collateral sulcus (ptCoS: hV4/VO1 boundary)	Lt. medial occipito-temporal sulcus	−4.111	0.37 (0.35)	0.23 (0.24)	0.49 (0.37)
16	Rt. inferior temporal gyrus	Rt. superior precentral sulcus	−4.048	0.44 (0.44)	0.20 (0.28)	0.48 (0.38)
17	Lt. pars orbitalis	Lt. parahippocampal gyrus	−4.044	0.51 (0.37)	0.21 (0.25)	0.47 (0.36)
18	Rt. medial occipito-temporal sulcus	Rt. medial orbital sulcus	−4.025	0.40 (0.38)	0.21 (0.28)	0.48 (0.35)
19	Lt. ACC	Lt. parahippocampal gyrus	−3.973	0.40 (0.36)	0.22 (0.28)	0.49 (0.37)
20	Lt. horizontal ramus of the anterior segment of the lateral sulcus	Lt. inferior frontal sulcus	−3.846	0.53 (0.38)	0.23 (0.22)	0.45 (0.34)
21	Rt. superior precentral sulcus	Lt. precentral gyrus	−3.828	0.26 (0.31)	0.26 (0.32)	0.56 (0.37)
22	Rt. Superior precentral sulcus	Lt. superior parietal lobule	−3.768	0.29 (0.31)	0.23 (0.26)	0.48 (0.37)
23	Rt. ACC	Lt. ACC	3.755	0.56 (0.33)	0.78 (0.26)	0.54 (0.33)

Abbreviations: ACC, anterior cingulate cortex; FEP-AH, first episode psychosis with auditory hallucination; FEP-NAH, first episode psychosis without auditory hallucination; HC, healthy control; LOOGC, leave-one-out group-comparison; L, left; R, Right.

abnormalities in FEP-AH subjects at the network level. Two subregions of Broca's complex [Xiang et al., 2010] - the left pars triangularis (BA 45) and left pars orbitalis (BA 47), both of which process semantic information – exhibited decreased CSA-ISC with the right IPS and left circular sulcus of the anterior insula (BA 13), respectively. Specifically, the CSA of the left frontal cortex is heavily influenced by genetic loading (about 76%) rather than by environmental factors (about 24%) [Eyler et al., 2011]. Considering the smaller degree of postnatal relative cortical expansion in inferior frontal cortices, greater expansion of cortex buried in sulci including IPS (specifically in FEP-AH patients) may result in a disproportionately weaker CSA-ISC between left pars triangularis and right IPS [Hill et al., 2010]. Of note, the IPS region not only regulates visuospatial attention and related eye movement but also generates self-originated intentions for action such as inner speech or thoughts [Ffytche and Wible, 2014]. Moreover, speech production (either vocal or subvocal), maintenance of verbal thought content in working memory and experience of self-agency for which action accompanies dual activation of right IPS and anterior insula [Ffytche and Wible, 2014].

ECN-Wernicke's Module Complex of CT-ISCs in FEP-AH

In FEP-AH subjects, a set of CT-ISCs constructed between right DLPFC-left angular gyrus-left middle temporal gyrus, among others, successfully demonstrated altered interaction of ECN [Seeley et al., 2007]-Wernicke's module [Tomasi and Volkow, 2012] complex during additional, disease-related cortical thinning [Clos et al., 2014]. The right superior frontal sulcus, which demarcates the upper portion of the DLPFC, revealed decreased CT-ISCs with the right middle frontal gyrus (DLPFC) and with left angular gyrus (which is also a key component of DMN). This prefrontal sulcus controls dimensional shifts of attention [Morton et al., 2009] and is involved in classification of familiar and unfamiliar stimuli [Thiel et al., 2014]. Moreover, development-related maturation of CT in core components of ECN, including the DLPFC and angular gyrus, are heavily influenced by genetic factors [Seeley et al., 2007] and disease (schizophrenia)-related changes [Tao et al., 2014]. Therefore, attenuated strength of CT-ISCs between these three brain areas of ECN, which also undergo accelerated cortical thinning during progression from a prodromal disease state to psychosis [Ziermans et al., 2012], could be related to dysfunctional executive control and faulty decision making in the context of self-generated semantic contents in FEP-AH subjects [Fletcher and Frith, 2009]. Furthermore, reminiscent of volumetric changes in the temporal cortex in children experiencing multiple, attenuated symptoms of psychosis before disease onset [Cullen et al., 2013], decreased CT-ISC between the left anterior occipital sulcus (an infero-

lateral border of occipital lobe) vs. left middle temporal gyrus (which form part of Wernicke's module in language network) [Tomasi and Volkow, 2012] in FEP-AH subjects also distinguished FEP-AH from FEP-NAH subjects successfully.

Abnormal CSA-ISC/CT-ISC Of Default-Mode Network in FEP

This study illustrated the disordered structure of the DMN in schizophrenia [Meda et al., 2014], reflected by alterations in the strength of cortical morphology-based ISCs in both FEP-AH and FEP-NAH subjects (Figs. 2 and 3 and **Tables IV-V**). From the perspective of inter-network communication between the DMN and other intrinsic brain networks [Manoliu et al., 2014], several CSA-ISCs and CT-ISCs characterizing FEP-AH or FEP-NAH from HC demonstrated overlapping patterns repetitively, including alteration of ISCs between the hub regions of DMN versus hub components of other intrinsic brain networks such as language network, ECN, salience network, dorsal attention network, auditory and visual network. Furthermore, we also detected dysfunctional network structure in the DMN itself [Bastos-Leite et al., 2015]: changes were observed in strength of ISC, not only between the two subsystems of DMN (the dorsal medial prefrontal cortex subsystem [temporal pole, sulcus intermedius primus of inferior parietal lobule; a subsystem of DMN mainly activated when individuals consider their current mental state] and the medial temporal lobe subsystem [precuneus, anterior cingulate cortex (ACC); activated preferentially during episodic decision about their future]), but also between hub regions of the medial temporal lobe subsystem (left parahippocampal gyrus vs. left suborbital sulcus and left ACC vs. right ACC) themselves [Andrews-Hanna et al., 2010].

Limitations

This study also has some limitations. First, there was significant group difference of IQ score between the FEP group and HCs (Table I). The possibility of lowered cognitive function, including IQ, of schizophrenic subjects must also be considered as a possible intermediate phenotype of proneness to psychosis [Woodberry et al., 2008], which might be difficult to dissociate from psychosis per se. Second, as our FEP subjects were prescribed with antipsychotics prior to MRI (Table I), additional changes of cortical thickness in response to the antipsychotics usage could not be excluded; however, the chances of changes in CSA under the influence of antipsychotics might be minimal [Gutierrez-Galve et al., 2015b]. Thirdly, although we tried to confirm the generalizability of our neuroanatomical decision function in classifying the FEP-AH from FEP-NAH or from HC across diverse compositions of dataset by way of the 10,000 cross-validation procedures, further studies to challenge the utility of our result onto the independent dataset recruited from other clinics are warranted.

CONCLUSION

In conclusion, we established herein a distinctive intermediate phenotype of biological proneness for AH using CSA-ISCs as well as disease state marker indicating the severity of AH using CT-ISCs. These selected features of individualized cortical covariance could successfully classify FEP-AHs from FEP-NAHs or HCs and could provide insights into the individualized focus of targeted neurointervention treatment approach. Future studies to reconfirm the generalizability of current finding in diverse clinical situations are required.

REFERENCES

Alexander-Bloch A, Giedd JN, Bullmore E (2013a): Imaging structural co-variance between human brain regions. Nat Rev Neurosci 14:322–336.

Alexander-Bloch A, Raznahan A, Bullmore E, Giedd J (2013b): The convergence of maturational change and structural covariance in human cortical networks. J Neurosci 33:2889–2899.

Anderson JS, Ferguson MA, Lopez-Larson M, Yurgelun-Todd D (2010): Topographic maps of multisensory attention. Proc Natl Acad Sci U S A 107:20110–20114.

Andreasen NC, Flaum M (1991): Schizophrenia: The characteristic symptoms. Schizophr Bull 17:27–49.

Andrews-Hanna JR, Reidler JS, Sepulcre J, Poulin R, Buckner RL (2010): Functional-anatomic fractionation of the brain's default network. Neuron 65:550–562.

Bastos-Leite AJ, Ridgway GR, Silveira C, Norton A, Reis S, Friston KJ (2015): Dysconnectivity within the default mode in first-episode schizophrenia: a stochastic dynamic causal modeling study with functional magnetic resonance imaging. Schizophr Bull 41:144–153.

Benetti S, Pettersson-Yeo W, Allen P, Catani M, Williams S, Barsaglini A, Kambeitz-Ilankovic LM, McGuire P, Mechelli A (2015): Auditory verbal hallucinations and brain dysconnectivity in the perisylvian language network: A multimodal investigation. Schizophr Bull 41:192–200.

Bruss GS, Gruenberg AM, Goldstein RD, Barber JP (1994): Hamilton Anxiety Rating Scale Interview guide: Joint interview and test-retest methods for interrater reliability. Psychiatry Res 53: 191–202.

Buckholtz JW, Meyer-Lindenberg A (2012): Psychopathology and the human connectome: Toward a transdiagnostic model of risk for mental illness. Neuron 74:990–1004.

Cachia A, Amad A, Brunelin J, Krebs MO, Plaze M, Thomas P, Jardri R (2015): Deviations in cortex sulcation associated with visual hallucinations in schizophrenia. Mol Psychiatry 20:1101–1107.

Cannon TD, Chung Y, He G, Sun D, Jacobson A, van Erp TG, McEwen S, Addington J, Bearden CE, Cadenhead K, Cornblatt B, Mathalon DH, McGlashan T, Perkins D, Jeffries C, Seidman LJ, Tsuang M, Walker E, Woods SW, Heinssen R, North American Prodrome Longitudinal Study Consortium (2015): Progressive Reduction in Cortical Thickness as Psychosis Develops: A

Multisite Longitudinal Neuroimaging Study of Youth at Elevated Clinical Risk. Biol Psychiatry 77:147–157.

Catani M, Craig MC, Forkel SJ, Kanaan R, Picchioni M, Toulopoulou T, Shergill S, Williams S, Murphy DG, McGuire P (2011): Altered integrity of perisylvian language pathways in schizophrenia: Relationship to auditory hallucinations. Biol Psychiatry 70:1143–1150.

Chen AC, Oathes DJ, Chang C, Bradley T, Zhou ZW, Williams LM, Glover GH, Deisseroth K, Etkin A (2013): Causal interactions between fronto-parietal central executive and default-mode networks in humans. Proc Natl Acad Sci U S A 110: 19944–19949.

Chi JG, Dooling EC, Gilles FH (1977): Gyral development of the human brain. Ann Neurol 1:86–93.

Clarkson MJ, Cardoso MJ, Ridgway GR, Modat M, Leung KK, Rohrer JD, Fox NC, Ourselin S (2011): A comparison of voxel and surface based cortical thickness estimation methods. Neuroimage 57:856–865.

Clos M, Diederen KM, Meijering AL, Sommer IE, Eickhoff SB (2014): Aberrant connectivity of areas for decoding degraded speech in patients with auditory verbal hallucinations. Brain Struct Funct 219:581–594.

Cullen AE, De Brito SA, Gregory SL, Murray RM, Williams SC, Hodgins S, Laurens KR (2013): Temporal lobe volume abnormalities precede the prodrome: A study of children presenting antecedents of schizophrenia. Schizophr Bull 39:1318–1327.

Destrieux C, Fischl B, Dale A, Halgren E (2010): Automatic parcellation of human cortical gyri and sulci using standard anatomical nomenclature. Neuroimage 53:1–15.

Dosenbach NU, Nardos B, Cohen AL, Fair DA, Power JD, Church JA, Nelson SM, Wig GS, Vogel AC, Lessov-Schlaggar CN, Barnes KA, Dubis JW, Feczko E, Coalson RS, Pruett JR, Jr., Barch DM, Petersen SE, Schlaggar BL (2010): Prediction of individual brain maturity using fMRI. Science 329:1358–1361.

Edgar CJ, Blaettler T, Bugarski-Kirola D, Le Scouiller S, Garibaldi GM, Marder SR (2014): Reliability, validity and ability to detect change of the PANSS negative symptom factor score in outpatients with schizophrenia on select antipsychotics and with prominent negative or disorganized thought symptoms. Psychiatry Res 218:219–224.

Eyler LT, Prom-Wormley E, Panizzon MS, Kaup AR, Fennema-Notestine C, Neale MC, Jernigan TL, Fischl B, Franz CE, Lyons MJ, Grant M, Stevens A, Pacheco J, Perry ME, Schmitt JE, Seidman LJ, Thermenos HW, Tsuang MT, Chen CH, Thompson WK, Jak A, Dale AM, Kremen WS (2011): Genetic and environmental contributions to regional cortical surface area in humans: A magnetic resonance imaging twin study. Cereb Cortex 21:2313–2321.

Ffytche DH, Wible CG (2014): From tones in tinnitus to sensed social interaction in schizophrenia: How understanding cortical organization can inform the study of hallucinations and psychosis. Schizophr Bull 40 Suppl 4:S305–S316.

Fischl B, Dale AM (2000): Measuring the thickness of the human cerebral cortex from magnetic resonance images. Proc Natl Acad Sci U S A 97:11050–11055.

Fischl B, van der Kouwe A, Destrieux C, Halgren E, Segonne F, Salat DH, Busa E, Seidman LJ, Goldstein J, Kennedy D, Caviness V, Makris N, Rosen B, Dale AM (2004): Automatically parcellating the human cerebral cortex. Cereb Cortex 14:11–22.

Fletcher PC, Frith CD (2009): Perceiving is believing: A Bayesian approach to explaining the positive symptoms of schizophrenia. Nat Rev Neurosci 10:48–58.

Gutierrez-Galve L, Chu EM, Leeson VC, Price G, Barnes TR, Joyce EM, Ron MA (2015a): A longitudinal study of cortical changes and their cognitive correlates in patients followed up after first-episode psychosis. Psychol Med 45:205–216.

Gutierrez-Galve L, Chu EM, Leeson VC, Price G, Barnes TR, Joyce EM, Ron MA (2015b): A longitudinal study of cortical changes and their cognitive correlates in patients followed up after first-episode psychosis. Psychol Med 45:205–216.

Hall RC (1995): Global assessment of functioning. A modified scale. Psychosomatics 36:267–275.

Haukvik UK, Rimol LM, Roddey JC, Hartberg CB, Lange EH, Vaskinn A, Melle I, Andreassen OA, Dale A, Agartz I (2014): Normal birth weight variation is related to cortical morphology across the psychosis spectrum. Schizophr Bull 40:410–419.

Hill J, Inder T, Neil J, Dierker D, Harwell J, Van Essen D (2010): Similar patterns of cortical expansion during human development and evolution. Proc Natl Acad Sci U S A 107:13135–13140.

Irimia A, Chambers MC, Torgerson CM, Van Horn JD (2012): Circular representation of human cortical networks for subject and population-level connectomic visualization. Neuroimage 60:1340–1351.

Jardri R, Pouchet A, Pins D, Thomas P (2011): Cortical activations during auditory verbal hallucinations in schizophrenia: A coordinate-based meta-analysis. Am J Psychiatry 168:73–81.

Jardri R, Thomas P, Delmaire C, Delion P, Pins D (2013): The neurodynamic organization of modality-dependent hallucinations. Cereb Cortex 23:1108–1117.

Kambeitz J, Kambeitz-Ilankovic L, Leucht S, Wood S, Davatzikos C, Malchow B, Falkai P, Koutsouleris N (2015): Detecting Neuroimaging Biomarkers for Schizophrenia: A Meta-Analysis of Multivariate Pattern Recognition Studies. Neuropsychopharmacology 40:1742–1751.

Kay SR, Fiszbein A, Opler LA (1987): The positive and negative syndrome scale (PANSS) for schizophrenia. Schizophr Bull 13: 261–276.

Kremen WS, Fennema-Notestine C, Eyler LT, Panizzon MS, Chen CH, Franz CE, Lyons MJ, Thompson WK, Dale AM (2013): Genetics of brain structure: Contributions from the Vietnam Era Twin Study of Aging. Am J Med Genet B Neuropsychiatr Genet 162B:751–761.

Krzywinski M, Schein J, Birol I, Connors J, Gascoyne R, Horsman D, Jones SJ, Marra MA (2009): Circos: An information aesthetic for comparative genomics. Genome Res 19:1639–1645.

Kubera KM, Sambataro F, Vasic N, Wolf ND, Frasch K, Hirjak D, Thomann PA, Wolf RC (2014): Source-based morphometry of gray matter volume in patients with schizophrenia who have persistent auditory verbal hallucinations. Prog Neuropsychopharmacol Biol Psychiatry 50:102–109.

Manoliu A, Riedl V, Zherdin A, Muhlau M, Schwerthoffer D, Scherr M, Peters H, Zimmer C, Forstl H, Bauml J, Wohlschlager AM, Sorg C (2014): Aberrant dependence of default mode/central executive network interactions on anterior insular salience network activity in schizophrenia. Schizophr. Bull 40:428–437.

Meda SA, Ruano G, Windemuth A, O'Neil K, Berwise C, Dunn SM, Boccaccio LE, Narayanan B, Kocherla M, Sprooten E, Keshavan MS, Tamminga CA, Sweeney JA, Clementz BA, Calhoun VD, Pearlson GD (2014): Multivariate analysis reveals genetic associations of the resting default mode network in psychotic bipolar disorder and schizophrenia. Proc Natl Acad Sci U S A 111:E2066–E2075.

Meier MH, Caspi A, Reichenberg A, Keefe RS, Fisher HL, Harrington H, Houts R, Poulton R, Moffitt TE (2014): Neuropsychological decline in schizophrenia from the premorbid to the postonset period: Evidence from a population-representative longitudinal study. Am J Psychiatry 171:91–101.

Menon V (2011): Large-scale brain networks and psychopathology: a unifying triple network model. Trends Cogn Sci 15:483–506.

Modinos G, Vercammen A, Mechelli A, Knegtering H, McGuire PK, Aleman A (2009): Structural covariance in the hallucinating brain: a voxel-based morphometry study. J Psychiatry Neurosci 34:465–469.

Morton JB, Bosma R, Ansari D (2009): Age-related changes in brain activation associated with dimensional shifts of attention: An fMRI study. Neuroimage 46:249–256.

Rubinov M, Knock SA, Stam CJ, Micheloyannis S, Harris AW, Williams LM, Breakspear M, Honey GD, Pomarol-Clotet E, Corlett PR, Honey RA, McKenna PJ, Bullmore ET, Fletcher PC, Friston KJ (2009): Small-world properties of nonlinear brain activity in schizophrenia. Hum Brain Mapp 30:403–416.

Russo M, Levine SZ, Demjaha A, Di Forti M, Bonaccorso S, Fearon P, Dazzan P, Pariante CM, David AS, Morgan C, Murray RM, Reichenberg A (2014): Association between symptom dimensions and categorical diagnoses of psychosis: A cross-sectional and longitudinal investigation. Schizophr Bull 40:111–119.

Sanabria-Diaz G, Melie-Garcia L, Iturria-Medina Y, Aleman-Gomez Y, Hernandez-Gonzalez G, Valdes-Urrutia L, Galan L, Valdes-Sosa P (2010): Surface area and cortical thickness descriptors reveal different attributes of the structural human brain networks. Neuroimage 50:1497–1510.

Seeley WW, Menon V, Schatzberg AF, Keller J, Glover GH, Kenna H, Reiss AL, Greicius MD (2007): Dissociable intrinsic connectivity networks for salience processing and executive control. J Neurosci 27:2349–2356.

Shergill SS, Brammer MJ, Williams SC, Murray RM, McGuire PK (2001): Mapping auditory hallucinations in schizophrenia using functional magnetic resonance imaging. Schizophr Res 49:186–186.

Tao R, Cousijn H, Jaffe AE, Burnet PW, Edwards F, Eastwood SL, Shin JH, Lane TA, Walker MA, Maher BJ, Weinberger DR, Harrison PJ, Hyde TM, Kleinman JE (2014): Expression of ZNF804A in human brain and alterations in schizophrenia, bipolar disorder, and major depressive disorder: A novel transcript fetally regulated by the psychosis risk variant rs1344706. JAMA Psychiatry 71:1112–1120.

Thiel CM, Studte S, Hildebrandt H, Huster R, Weerda R (2014): When a loved one feels unfamiliar: A case study on the neural basis of Capgras delusion. Cortex 52:75–85.

Tomasi D, Volkow ND (2012): Resting functional connectivity of language networks: characterization and reproducibility. Mol Psychiatry 17:841–854.

Valk SL, Di Martino A, Milham MP, Bernhardt BC (2015): Multicenter mapping of structural network alterations in autism. Hum Brain Mapp 36:2364–2373.

van Lutterveld R, van den Heuvel MP, Diederen KM, de Weijer AD, Begemann MJ, Brouwer RM, Daalman K, Blom JD, Kahn RS, Sommer IE (2014): Cortical thickness in individuals with non-clinical and clinical psychotic symptoms. Brain 137:2664–2669.

van Waarde JA, Scholte HS, van Oudheusden LJ, Verwey B, Denys D, van Wingen GA (2015): A functional MRI marker may predict the outcome of electroconvulsive therapy in severe and treatment-resistant depression. Mol Psychiatry 20:609–614.

Wee CY, Yap PT, Shen D, Alzheimer's Disease Neuroimaging I (2013): Prediction of Alzheimer's disease and mild cognitive impairment using cortical morphological patterns. Hum Brain Mapp 34:3411–3425.

Wheeler AL, Chakravarty MM, Lerch JP, Pipitone J, Daskalakis ZJ, Rajji TK, Mulsant BH, Voineskos AN (2014): Disrupted prefrontal interhemispheric structural coupling in schizophrenia related to working memory performance. Schizophr Bull 40: 914–924.

Woodberry KA, Giuliano AJ, Seidman LJ (2008): Premorbid IQ in schizophrenia: A meta-analytic review. Am J Psychiatry 165: 579–587.

Woods SW (2003): Chlorpromazine equivalent doses for the newer atypical antipsychotics. J Clin Psychiatry 64:663–667.

Xiang HD, Fonteijn HM, Norris DG, Hagoort P (2010): Topographical Functional Connectivity Pattern in the Perisylvian Language Networks. Cerebral Cortex 20:549–560.

Yum TH, Park YS, Oh KJ, Kim JG, Lee HY. (1992) The manual of Korean-Wechsler Adult Intrelligence Scale. Seoul: Korean Guidance Press.

Yun JY, Jang JH, Kim SN, Jung WH, Kwon JS (2015): Neural correlates of response to pharmacotherapy in obsessive-compulsive disorder: Individualized cortical morphology-based structural covariance. Prog Neuropsychopharmacol Biol Psychiatry 63:126–133.

Zielinski BA, Gennatas ED, Zhou J, Seeley WW (2010): Network-level structural covariance in the developing brain. Proc Natl Acad Sci U S A 107:18191–18196.

Ziermans TB, Schothorst PF, Schnack HG, Koolschijn PC, Kahn RS, van Engeland H, Durston S (2012): Progressive structural brain changes during development of psychosis. Schizophr Bull 38:519–530.

Zimmerman M, Martinez JH, Young D, Chelminski I, Dalrymple K (2013): Severity classification on the Hamilton Depression Rating Scale. J Affect Disord 150:384–388.